Vibroarthrographic Signal Classification for Knee Joint Disorder Detection using Tunable Q-factor Wavelet Transform based on Entropy Measures

Krishna Sundeep Basavaraju
National Institute of Technology Warangal, India
bs721065@student.nitw.ac.in (corresponding author)

T. Kishore Kumar
National Institute of Technology Warangal, India
kishoret@nitw.ac.in

K. Ashoka Reddy
Kakatiya Institute of Technology & Science Warangal, India
kareddy.iitm@gmail.com

Received: 12 October 2024 | Revised: 6 November 2024 | Accepted: 12 December 2024

 DOI: https://doi.org/10.48084/etasr.9245

ABSTRACT

Research on Vibroarthrographic (VAG) signals presents a promising means for the early diagnosis of knee joint disorders. However, the classification problem for these signals faces serious issues due to their complex and dynamic nature. This study proposes a novel method for decomposing and analyzing VAG signals based on a Tunable Q-factor Wavelet Transform (TQWT) and entropy-based measures. TQWT is used to preprocess and decompose VAG signals recorded during knee motion into subbands. Different entropy metrics, such as approximate entropy, sample entropy, fuzzy entropy, slope entropy, and so on, were computed over different subbands of the signal to capture significant signal features. Effective features were selected using Recursive Feature Elimination (RFE) and then classified using ensemble classifiers such as XGBoost, Ensemble Random Forest (ERF), and RF-logistic regression. The classification accuracy of the proposed sample entropy method was 87.64% and had 90% sensitivity, 86.36% specificity, and 0.88 AUC-ROC. These results demonstrate the ability of the TQWT-based approach to discriminate knee joint abnormalities. Future work will explore performance scaling with larger datasets and apply it to other joint disorders.

Keywords-VAG signal; tunable Q-factor wavelet transform; feature extraction; classifiers

I. INTRODUCTION

The knee condition causes extreme discomfort that prevents walking or weight on the knee. Without prompt treatment, knee dysfunction causes Osteoarthritis (OA) [1, 2]. Almost 3% of people worldwide have knee disorders, leading to years lived with disability. In addition, knee disease ranks fourth among YLDs. Knee issues are common in early aging, especially in low-income countries [3], and rural hospitals lack medical imaging and technological innovation equipment. Modern medical technology uses computer methods to diagnose human skeletal models. OA and Chondromalacia patella are the main knee diseases from phase I to IV. Invasive and non-invasive procedures are used to estimate clinical and operational performance. However, diagnosing knee disorders with X-rays, MRI, ultrasonography, CT, and other imaging methods is expensive [4, 5]. Recent knee joint diagnosis uses non-invasive vibration signal detection technologies called Vibroarthrography (VAG) to detect problems. VAG is a promising screening method that analyzes knee vibrations extracted during movement. These signals can be recorded using tiny industrial accelerometers, piezoelectric microphones, or electronic stethoscopes [6]. The extracted signals help identify the knee joint as normal or degenerative. Healthcare professionals can assess knee joint injury by evaluating signal frequency and amplitude fluctuations. Signal frequency and amplitude depend on the condition of the knee. Figure 1 shows normal and aberrant VAG signals. As VAG signal characteristics are difficult to notice and analyze using simple amplitude and frequency notations, their internals must be

examined for knee joint features. In [7], abnormalities were detected and classified using time and spectral domain features. VAG signals were used to evaluate skewness, kurtosis, crest, margin, impulse, and shape factors. Signal decomposition and spectral properties, such as mean, peak, slope, flux, skewness, and kurtosis, were recovered using the Short-Time Fourier transform (STFT). In [8], complete ensemble empirical mode decomposition and HHT were used, obtaining 88.76% accuracy. This study extracted statistical information from subband temporal frequency images. Wavelet decomposition was used on VAG signals, features were calculated via recurrence quantification analysis, and approximate, sample, and wavelet-based subband entropies were determined.

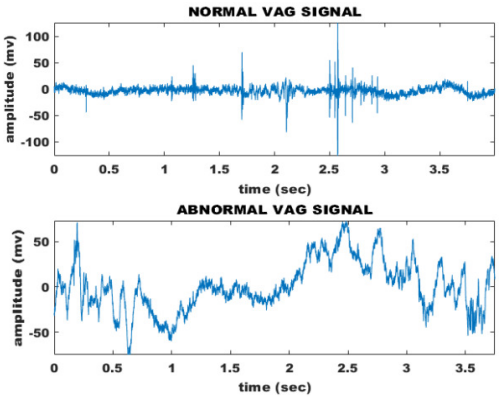

Fig. 1. VAG signals: normal and abnormal.

Artifacts consistently interfere with VAG signals during recording. Various signal decomposition methods, such as Empirical Mode Decomposition (EMD) and its enhanced variants, EEMD and CEEMDAN, have been employed to assess and remove subbands that induce random noise [9]. Signal reconstruction by EMD involves the identification of subbands, called Intrinsic Mode Functions (IMFs), employing Detrended Fluctuation Analysis (DFA) and selecting suitable IMFs within the interval of $0 < \alpha < 1.5$ [10]. In [11], TQWT was used to decompose VAG signals into various subbands. The Q factor ranged from 2 to 31 and the decomposition was 50. Using synthetic minority oversampling with TQWT, an accuracy of 80.89% was achieved. In [12], Kroskov entropy and fractal dimension features were extracted from decomposed subbands using TQWT for VAG signal decomposition, achieving 86.91% accuracy using the least square support vector machine classifier. In [13], an effective actigraphy-based VAG data encoding and analysis system was proposed. This method measures cartilage deterioration and identifies limb movement cracking. Encoding the data into three bits per sample compresses it without sacrificing limb movement information, achieving 84.6% recognition accuracy. This efficient data compression simplifies the transmission and storage of VAG data. In [14], VAG signals were partitioned into subbands using DDDTCWT. The L2 norms and log energy entropy were retrieved from these subbands. Differentiating normal from aberrant VAG signals required these features. This study used Fuzzy Sugeno Classifier (FSC), Least Squares Support Vector Machine (LS-SVM), and sequential minimal optimization SVM to classify VAG signals using ten-fold cross-validation, achieving 85.39% classification accuracy. The study in [15] examined how sensor placement affected data collection and accuracy due to movement changes and knee joint load effect, helping to analyze knee movements and disorder severity during daily activities.

II. METHOD

Due to knee movement during signal capture, VAGs are always contaminated by Baseline Wandering (BLW). A VAG signal Cascaded Moving Average (CMA) filter reduces this low-frequency quasiperiodic BLW [16]. This VAG signal collection approach is painless and non-invasive in diagnosing knee joint problems. Fixing the accelerometer sensor to the mid-patella yields VAG signals. These signals are captured during leg extension and flexion movements from 135° to 0° and 0° to 135°. The signal was prefiltered and amplified with a 10 Hz - 1 kHz bandpass filter. A 2 kHz sampling rate and 12-bit digitization were used.

$$y(i) = \frac{1}{2P}\sum_{p=1}^{P} x(i-p) + \frac{1}{2Q}\sum_{q=1}^{Q} x(i-P+O-q) \quad (1)$$

where P denotes the order of the first-stage filter, Q signifies the order of the second filter, and O indicates the number of overlapping samples taken into account. This study examined a two-stage filter with parameters $P = Q = 20$ and an overlap of $O = 5$ samples. Figure 2 illustrates the process of VAG signal classification for knee joint diseases. The processes involved are (i) Preprocessing, (ii) Signal decomposition utilizing TQWT, (iii) Entropy-based feature extraction, (iv) feature selection, and (v) classification.

A. *Tunable Q-factorWavelet Transform (TQWT)*

The TQWT technique is a multiresolution analysis method where the Q factor can be specified by the user. The flexibility of adjusting the Q value leads to the design of various filters for specific spectral decomposition [17]. The filter designs depend on low- and high-pass filter bands viz., $H_0^J(\omega)$ and $H_1^J(\omega)$. The filter parameters, α for low pass scaling and β for high pass scaling, are in turn estimated from the Q value, redundancy (r), and total decomposition level (J) [19].

$$H_0^J(\omega) = \begin{cases} \prod_{m=0}^{J-1} H_0\left(\frac{\omega}{\alpha^m}\right), & |\omega| \le \alpha^J\pi \\ 0, & \alpha^J\pi \le |\omega| \le \pi \end{cases} \quad (2)$$

$$H_0^J(\omega) = \begin{cases} H_1\left(\frac{\omega}{\alpha^{J-1}}\right)\prod_{m=0}^{J-2} H_0\left(\frac{\omega}{\alpha^m}\right), \\ (1-\beta)\alpha^{J-1}\pi \le |\omega| \le \alpha^J\pi \\ 0, \text{ for other } \epsilon\,[-\pi,\pi] \end{cases} \quad (3)$$

$$H_0(\omega) = \theta\left(\frac{\omega+(\beta-1)\pi}{\alpha+\beta-1}\right) \quad (4)$$

$$H_1(\omega) = \theta\left(\frac{\alpha\pi-\omega}{\alpha+\beta-1}\right) \quad (5)$$

where $\theta(\omega)$ is the Daubechies filter's frequency response:

$$\theta(\omega) = 0.5(1+\cos(\omega))\sqrt{2-\cos(\omega)} \quad (6)$$

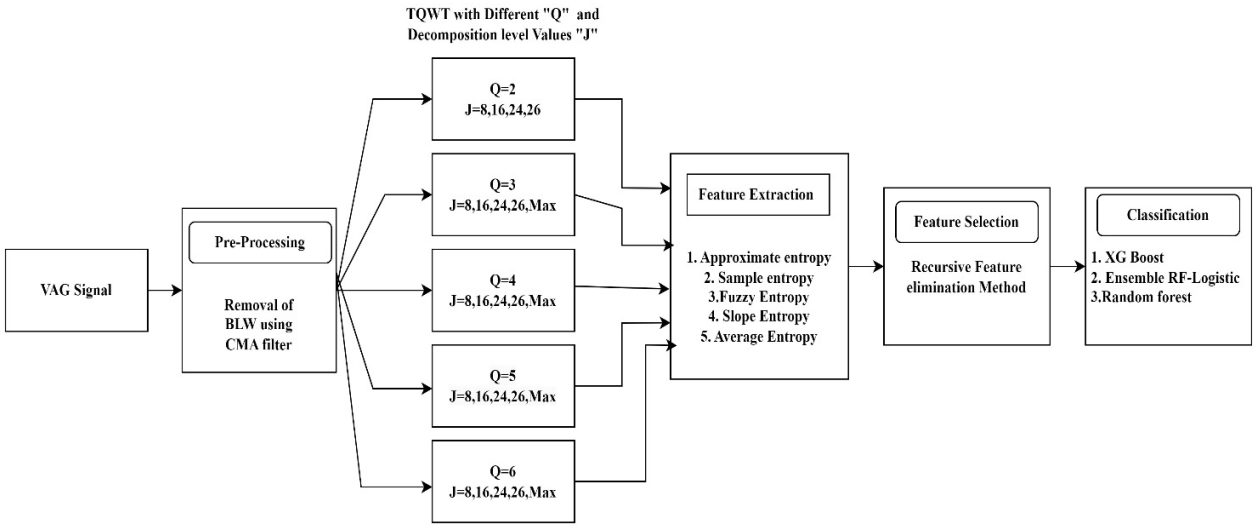

Fig. 2. VAG signal classification for knee joint disorders.

The interrelation among the low- and high-pass scaling parameters, and redundancy, α, β, r, Q and J are given as follows:

$$r = \frac{\beta}{\alpha - 1} \quad (7)$$

$$Q = \frac{2-\beta}{\beta} \quad (8)$$

$$J = \frac{log\left(\frac{\beta N}{8}\right)}{log\left(\left(\frac{1}{\alpha}\right)\right)} \quad (9)$$

The pre-processed VAG signals are segmented into subbands using TQWT. Figure 3 shows some of the subbands decomposed for abnormal VAG signals.

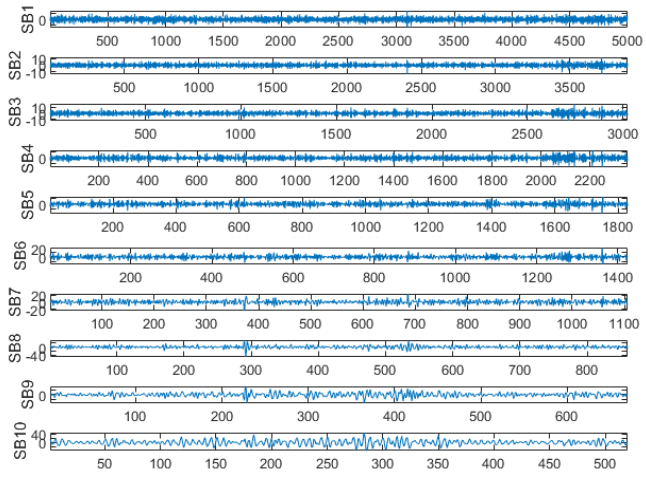

Fig. 3. TQWT generated subbands (1 to 10) of abnormal VAG signal.

This study focuses on examining VAG signals with respect to variation in Q value in TQWT and also the decomposition level J variation. This study considered the Q values from 2 to 6, J as 8, 16, 24, 26, and the maximum possible decomposition level with respect to Q, i.e., if Q = 2 leads to the maximum decomposition level J = 26, Q = 3 leads to J = 33, Q = 4 leads to J = 41, Q = 5 leads to J = 49, and Q = 6 leads to J = 56.

III. RESULTS

The dataset used comprised 89 VAG signals, including 51 from normal knees and 38 from aberrant knees [18]. VAG signals are consistently compromised by BLW and random noise, as shown in Figure 4. VAG signals require preprocessing to remove artifacts and improve classification. BLW from the VAG signal was diminished using a CMA filter of order 20 at each stage, utilizing five overlapping samples. Figures 6 and 7 display VAG signals before and after CMA filtering with parameters P = 20, Q = 20, and O = 5. After this, TQWT decomposes BLW artifact-free signals into subbands. Only ten information subbands are shown in Figure 5. The approximation, sample, fuzzy, slope, and average entropies were computed [19-24] for all subbands and all signals in the dataset, for different Q (Q: 2, 3, 4, 5, 6) and J values (J: 8, 16, 24, 26, maximum decomposition obtained for specific Q) subbands. Classification accuracy depends on feature quality.

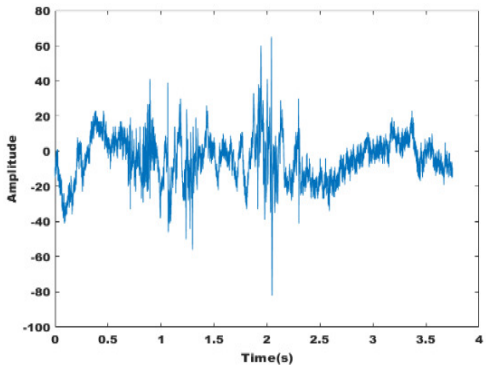

Fig. 4. VAG signal with BLW.

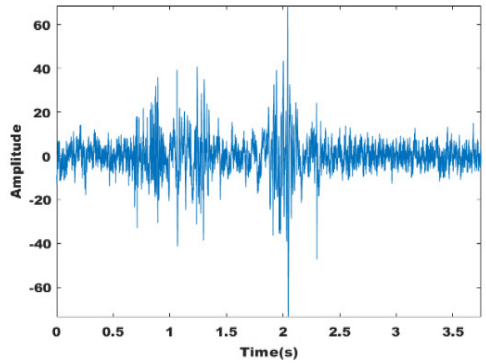

Fig. 5. Preprocessed VAG signal after applying CMA filter for BLW.

Recursive Feature Elimination (RFE) was used to find prominent traits that distinguish normal from abnormal situations. Using RFE, the three most influential subbands were found for each entropy. Table I shows the RFE-selected subbands for all entropies. These features was validated using XGBoost (XGB), Ensemble Ensemble RF-Logistic (ERFL), and Random Forest (RF), trained on 80% and tested on 20% of the dataset. Table II shows the highest accuracy for each entropy and other classifier evaluation criteria. The proposed VAG signal classification approach was evaluated utilizing performance metrics such as accuracy (Acc), Sensitivity (Sen), Specificity (Spe), Precision, F1 score, Area Under the Curve (AUC), Matthews Correlation Coefficient (MCC), Positive Predictive Value (PPV), and Negative Predictive Value (NPV). Table II presents the classification results. The proposed entropy-based TQWT technique yielded the best results in detecting abnormalities using XGBoost, Ensemble RF-Logistic (ERFL), and Random Forest (RF). Among the eleven entropies, approximate, sample, fuzzy, slope, and average entropies yielded the most favorable results. Table III compares these results with previous works.

TABLE I. RFE-SELECTED SUB-BANDS FOR ALL ENTROPIES

Entropy	***J***	***Q* = 2**	***Q* = 3**	***Q* = 4**	***Q* = 5**	***Q* = 6**
Appr EN	8	SB1, SB7, SB8	SB1, SB6, SB7	SB1, SB2, SB8	SB1, SB5, SB8	SB2, SB3, SB8
	16	SB1, SB13, SB16	SB2, SB11, SB15	SB1, SB3, SB15	SB1, SB5, SB16	SB1, SB3, SB16
	24	SB1, SB10, SB15	SB2, SB11, SB15	SB1, SB14, SB17	SB1, SB18, SB23	SB1, SB3, SB24
	26	SB5, SB10, SB15	SB2, SB11, SB15	SB2, SB15, SB23	SB18, SB23, SB25	SB12,SB17, SB24
	MAX	-	SB1, SB11, SB15	SB3, SB19, SB28	SB1, SB20, SB23	SB2, SB27, SB41
SAMPEN	8	SB1, SB7, SB8	SB1, SB2, SB8	SB1, SB2, SB7	SB1, SB3, SB4	SB1, SB2, SB5
	16	SB7, SB10, SB15	SB1, SB11, SB14	SB1, SB15, SB16	SB1, SB2, SB16	SB1, SB15, SB24
	24	SB7, SB10, SB15	SB1, SB12, SB21	SB1, SB19, SB24	SB2, SB18, SB23	SB1, SB2, SB14
	26	SB1, SB8, SB16	SB1, SB11, SB15	SB1, SB15, SB25	SB1, SB20, SB23	SB2, SB5, SB21
	MAX	-	SB1, SB11, SB14	SB1, SB15, SB26	SB3, SB18, SB34	SB2, SB27, SB40
FUZZY EN	8	SB1, SB5, SB8	SB1, SB6, SB7	SB1, SB3, SB8	SB1, SB2, SB4	SB1, SB2, SB4
	16	SB1, SB13, SB15	SB1, SB6, SB12	SB1, SB5, SB16	SB1, SB2, SB11	SB1, SB2, SB11
	24	SB1, SB15, SB22	SB2, SB12, SB23	SB1, SB19, SB24	SB1, SB4, SB24	SB1, SB4, SB24
	26	SB1, SB13, SB15	SB1, SB11, SB25	SB1, SB15, SB19	SB1, SB23, SB18	SB1, SB23, SB24
	MAx	-	SB1, SB26, SB27	SB2, SB24, SB39	SB23, SB34, SB42	SB22,SB27, SB52
SLOPE EN	8	SB1, SB6, SB8	SB1, SB3, SB8	SB1, SB3, SB7	SB1, SB2, SB8	SB1, SB5, SB6
	16	SB1, SB14, SB16	SB1, SB3, SB13	SB1, SB8, SB15	SB1, SB2, SB8	SB1, SB10, SB15
	24	SB1, SB16, SB21	SB1, SB11, SB20	SB1, SB2, SB15	SB7, SB14, SB18	SB1, SB10, SB24
	26	SB1, SB16, SB23	SB1, SB11, SB20	SB1, SB3, SB15	SB1, SB4, SB18	SB1, SB10, SB24
	MAX	-	SB2, SB11, SB28	SB1, SB3, SB15	SB14, SB18, SB38	SB1, SB27, SB31
AVEN	8	SB1, SB4, SB7	SB1, SB7, SB8	SB1, SB3, SB8	SB1, SB2, SB8	SB1, SB6, SB8
	16	SB1, SB4, SB14	SB2, SB11, SB14	SB2, SB14, SB16	SB1, SB2, SB16	SB1, SB2, SB15
	24	SB1, SB4, SB12	SB1, SB11, SB24	SB1, SB14, SB22	SB1, SB16, SB17	SB1, SB15, SB21
	26	SB1, SB8, SB12	SB1, SB11, SB24	SB14, SB17, SB22	SB2, SB16, SB25	SB1, SB15, SB26
	MAX	-	SB1, SB11, SB24	SB1, SB14, SB32	SB1, SB16, SB29	SB1, SB21, SB41

TABLE II. CLASSIFIERS' PERFORMANCE FOR THE HIGHEST ACCURACIES RECORDED IN EACH ENTROPY

Feature	**Classifier**	**Acc**	**Sen**	**Spec**	**Pre**	**F1 score**	**AUC**	**MCC**	**PPV**	**NPV**
APEN Q=2,J=24	XG Boost	0.85359	0.81786	0.88	0.84167	0.82885	0.8489	0.7015	0.8417	0.8636
	En RF-logistic	0.80784	0.8	0.82182	0.8	0.77717	0.8109	0.6433	0.8	0.8672
	Random Forest	0.81961	0.825	0.82182	0.80069	0.79411	0.8234	0.6614	0.8007	0.8771
SAMPEN Q=6, J=24	XG Boost	0.87647	0.9	0.86364	0.83333	0.85756	0.8818	0.7622	0.8333	0.9278
	En RF-logistic	0.8098	0.71786	0.88364	0.83143	0.75835	0.8008	0.6214	0.8314	0.8123
	Random Forest	0.82092	0.8	0.84364	0.77778	0.7639	0.8218	0.6468	0.7778	0.8756
FUZZY EN Q=6 J=24	XG Boost	0.87582	0.84643	0.9	0.88286	0.85599	0.8732	0.7607	0.8829	0.8924
	En RF-logistic	0.87516	0.79286	0.94	0.93333	0.84656	0.8664	0.7623	0.9333	0.8607
	Random Forest	0.84183	0.78929	0.88182	0.85556	0.80906	0.8356	0.69	0.8556	0.8551
SLOPE EN Q=4 J=24	XG Boost	0.86471	0.87143	0.86182	0.85688	0.84507	0.8666	0.753	0.8569	0.9175
	En RF-logistic	0.83203	0.79286	0.86182	0.82768	0.79177	0.8273	0.6763	0.8277	0.8718
	Random Forest	0.85425	0.84286	0.86182	0.83434	0.82679	0.8523	0.7185	0.8343	0.8543
AVEN Q=6 J=56	XG Boost	0.83137	0.77143	0.88182	0.84643	0.78806	0.8266	0.6757	0.8464	0.8541
	En RF-logistic	0.83072	0.71429	0.92	0.90833	0.77219	0.8171	0.6785	0.9083	0.8242
	Random Forest	0.86405	0.81786	0.9	0.88889	0.84218	0.8589	0.7375	0.8889	0.8694

TABLE III. ENHANCED KNEE JOINT DISORDER CLASSIFICATION USING TQWT-BASED ENTROPY MEASURES AND ENSEMBLE CLASSIFIERS

Source	Method	Features	Classification model	Evaluation Metric (%)
[8]	CEEMDAN	Entropy measures – ApEn, SampEn, PeEn, TsEn, ReEn, ShEn	LS-SVM	Acc: 86.61
[9]	-	Symbolic Entropy (SyEn), Approximate Entropy (ApEn), Fuzzy Entropy (FuzzyEn), and the mean, standard deviation, and Root-Mean-Squared (RMS) values of the envelope amplitude	SVM	Acc: 83.56
[13]	-	Statistical time and frequency features, band power, spiky index	SVM, LDA	Acc: 84.60
[14]	DDDTCWT	L2 norms and Log Energy Entropy (LEE)	Fuzzy Sugeno Classifier (FSC)	Acc: 85.39
[26]	EMD & CWT	Frequency domain features: CWT coefficients Spatiotemporal features: skewness and kurtosis of the autocorrelation function	LS-SVM	Acc: 86.67
[25]	EWT	Statistical Measures	SVM	Acc:83.33, Sen: 84.6, Spe: 80.0, Auc: 84.4
[27]	-	Normalized frequency features	SVM	Acc: not specified, Sen: 80.0
Proposed work	TQWT	Approximate Entropy, Sample Entropy, Fuzzy Entropy, Slope Entropy, Average Shannon Entropy	XGB, RF, Ensemble RF-logistic classifier	Acc: 87.64, Sen:0.9, Spe:0.8636, Auc:0.8818

The proposed TQWT-based method achieved 87.64% accuracy, 90.00% sensitivity, and 86.36% specificity. Further support for the performance of the method comes from a high MCC of 76.21, indicating that the model is capable of properly distinguishing between normal and abnormal knee joints. Additionally, the Area Under the Curve (AUC) value of 88.18 shows that the proposed approach is also capable of correctly classifying knee joint disorders, indicating its prediagnostic ability in clinical contexts.

This study focused on classifying knee joint disorders using VAG signals analyzed using the TQWT method. By using advanced entropy-based features along with XGBoost, ERF, and RF-logistic classifier, the overall accuracy was 87.64%. The results of this method had high sensitivity (90%) and specificity (86.36%) for the classification of knee joint disorders in the late stage of the disease using asymptomatic changes in the early stage. The integration of the RFE procedure to select the most expressive features for classification results in a gain in overall performance.

IV. CONCLUSION

This study presented a novel approach to process and categorize VAG signals acquired from knee joints to diagnose knee joint diseases at an early stage. The designed method focuses on the shift of VAG signals utilizing TQWT with entropy-based measures for the decomposition of signals. Comparing and contrasting various entropy measures including approximate entropy, sample entropy, fuzzy entropy, slope, and average entropies can determine some of the most efficient parameters for signal illustrations at various scientific measures of decomposition (J) and Q-factor levels. Based on RFE, the most important features that can distinguish between normal and abnormal knee conditions were chosen and then classified using ensemble RF, XGBoost, and LR classifiers. The proposed method attained an accuracy of 87.64%, a sensitivity of 90%, a specificity of 86.36%, and an AUC-ROC of 0.88 using sample entropy.

ACKNOWLEDGEMENT

This research work is supported by the Science and Engineering Research Board (SERB) Govt. of India under Grant no. CRG/2021/004501.

REFERENCES

[1] A. Cui, H. Li, D. Wang, J. Zhong, Y. Chen, and H. Lu, "Global, regional prevalence, incidence and risk factors of knee osteoarthritis in population-based studies," *eClinicalMedicine*, vol. 29, Dec. 2020, https://doi.org/10.1016/j.eclinm.2020.100587.

[2] V. P. Leifer, J. N. Katz, and E. Losina, "The burden of OA-health services and economics," *Osteoarthritis and Cartilage*, vol. 30, no. 1, pp. 10–16, Jan. 2022, https://doi.org/10.1016/j.joca.2021.05.007.

[3] B. Antony, G. Jones, X. Jin, and C. Ding, "Do early life factors affect the development of knee osteoarthritis in later life: a narrative review," *Arthritis Research & Therapy*, vol. 18, no. 1, Sep. 2016, Art. no. 202, https://doi.org/10.1186/s13075-016-1104-0.

[4] D. T. Felson, "Arthroscopy as a treatment for knee osteoarthritis," *Best Practice & Research Clinical Rheumatology*, vol. 24, no. 1, pp. 47–50, Feb. 2010, https://doi.org/10.1016/j.berh.2009.08.002.

[5] P. M. M. Cashman, R. I. Kitney, M. A. Gariba, and M. E. Carter, "Automated techniques for visualization and mapping of articular cartilage in MR images of the osteoarthritic knee: a base technique for the assessment of microdamage and submicro damage," *IEEE Transactions on NanoBioscience*, vol. 1, no. 1, pp. 42–51, Mar. 2002, https://doi.org/10.1109/TNB.2002.806916.

[6] R. M. Rangayyan, S. Krishnan, G. D. Bell, C. B. Frank, and K. O. Ladly, "Parametric representation and screening of knee joint vibroarthrographic signals," *IEEE Transactions on Biomedical Engineering*, vol. 44, no. 11, pp. 1068–1074, Aug. 1997, https://doi.org/10.1109/10.641334.

[7] M. M. Shidore, S. S. Athreya, S. Deshpande, and R. Jalnekar, "Screening of knee-joint vibroarthrographic signals using time and spectral domain features," *Biomedical Signal Processing and Control*, vol. 68, Jul. 2021, Art. no. 102808, https://doi.org/10.1016/j.bspc.2021.102808.

[8] S. Nalband, A. Prince, and A. Agrawal, "Entropy-based feature extraction and classification of vibroarthographic signal using complete ensemble empirical mode decomposition with adaptive noise," *IET Science, Measurement & Technology*, vol. 12, no. 3, pp. 350–359, 2018, https://doi.org/10.1049/iet-smt.2017.0284.

[9] Y. Wu *et al.*, "Quantification of knee vibroarthrographic signal irregularity associated with patellofemoral joint cartilage pathology based on entropy and envelope amplitude measures," *Computer Methods and Programs in Biomedicine*, vol. 130, pp. 1–12, Jul. 2016, https://doi.org/10.1016/j.cmpb.2016.03.021.

[10] Y. Wu, Knee Joint Vibroarthrographic Signal Processing and Analysis. Springer, 2015.

[11] E. Mascarenhas, S. Nalband, A. R. J. Fredo, and A. A. Prince, "Analysis and Classification of Vibroarthrographic Signals using Tuneable 'Q' Wavelet Transform," in *2020 7th International Conference on Signal Processing and Integrated Networks (SPIN)*, Noida, India, Feb. 2020, pp. 65–70, https://doi.org/10.1109/SPIN48934.2020.9071335.

[12] J. Zala, M. Sharma, and R. Bhalerao, "Tunable Q - wavelet transform based features for automated screening of knee-joint vibroarthrographic signals," in *2018 5th International Conference on Signal Processing and Integrated Networks (SPIN)*, Noida, India, Feb. 2018, pp. 348–352, https://doi.org/10.1109/SPIN.2018.8474117.

[13] Y. Athavale and S. Krishnan, "A telehealth system framework for assessing knee-joint conditions using vibroarthrographic signals," *Biomedical Signal Processing and Control*, vol. 55, Jan. 2020, Art. no. 101580, https://doi.org/10.1016/j.bspc.2019.101580.

[14] M. Sharma, P. Sharma, R. B. Pachori, and V. M. Gadre, "Double Density Dual-Tree Complex Wavelet Transform-Based Features for Automated Screening of Knee-Joint Vibroarthrographic Signals," in *Machine Intelligence and Signal Analysis*, 2019, pp. 279–290, https://doi.org/10.1007/978-981-13-0923-6_24.

[15] R. E. Andersen, L. Arendt-Nielsen, and P. Madeleine, "Knee joint vibroarthrography of asymptomatic subjects during loaded flexion-extension movements," *Medical & Biological Engineering & Computing*, vol. 56, no. 12, pp. 2301–2312, Dec. 2018, https://doi.org/10.1007/s11517-018-1856-6.

[16] S. Cai *et al.*, "Detrending knee joint vibration signals with a cascade moving average filter," in *2012 Annual International Conference of the IEEE Engineering in Medicine and Biology Society*, San Diego, CA, USA, Aug. 2012, pp. 4357–4360, https://doi.org/10.1109/EMBC.2012.6346931.

[17] I. W. Selesnick, "Wavelet Transform With Tunable Q-Factor," *IEEE Transactions on Signal Processing*, vol. 59, no. 8, pp. 3560–3575, Dec. 2011, https://doi.org/10.1109/TSP.2011.2143711.

[18] S. Krishnan, R. M. Rangayyan, G. D. Bell, C. B. Frank, and K. O. Ladly, "Adaptive filtering, modelling and classification of knee joint vibroarthrographic signals for non-invasive diagnosis of articular cartilage pathology," *Medical and Biological Engineering and Computing*, vol. 35, no. 6, pp. 677–684, Nov. 1997, https://doi.org/10.1007/BF02510977.

[19] S. M. Pincus, "Approximate entropy as a measure of system complexity.," *Proceedings of the National Academy of Sciences*, vol. 88, no. 6, pp. 2297–2301, Mar. 1991, https://doi.org/10.1073/pnas.88.6.2297.

[20] M. W. Flood and B. Grimm, "EntropyHub: An open-source toolkit for entropic time series analysis," *PLOS ONE*, vol. 16, no. 11, 2021, Art. no. e0259448, https://doi.org/10.1371/journal.pone.0259448.

[21] W. Chen, Z. Wang, H. Xie, and W. Yu, "Characterization of Surface EMG Signal Based on Fuzzy Entropy," *IEEE Transactions on Neural Systems and Rehabilitation Engineering*, vol. 15, no. 2, pp. 266–272, Jun. 2007, https://doi.org/10.1109/TNSRE.2007.897025.

[22] D. Cuesta-Frau, "Slope Entropy: A New Time Series Complexity Estimator Based on Both Symbolic Patterns and Amplitude Information," *Entropy*, vol. 21, no. 12, Dec. 2019, Art. no. 1167, https://doi.org/10.3390/e21121167.

[23] C. F. Hsu, S. Y. Wei, H. P. Huang, L. Hsu, S. Chi, and C. K. Peng, "Entropy of Entropy: Measurement of Dynamical Complexity for Biological Systems," *Entropy*, vol. 19, no. 10, Oct. 2017, Art. no. 550, https://doi.org/10.3390/e19100550.

[24] A. Amraoui and S. Saadi, "A Novel Approach on Speaker Gender Identification and Verification Using DWT First Level Energy and Zero Crossing," *Engineering, Technology & Applied Science Research*, vol. 12, no. 6, pp. 9570–9578, Dec. 2022, https://doi.org/10.48084/etasr.5269.

[25] K. S. Basavaraju, T. K. Kumar, K. A. Reddy, and K. R. K. Reddy, "Analysis of Vibroarthrographic signals for classification of knee disorders using Empirical Wavelet Transform based on Statistical measures," in *2023 IEEE International Instrumentation and Measurement Technology Conference (I2MTC)*, Kuala Lumpur, Malaysia, May 2023, pp. 1–6, https://doi.org/10.1109/I2MTC53148.2023.10175958.

[26] R. Gong, K. Hase, H. Goto, K. Yoshioka, and S. Ota, "Knee osteoarthritis detection based on the combination of empirical mode decomposition and wavelet analysis," *Journal of Biomechanical Science and Engineering*, vol. 15, no. 3, 2020, https://doi.org/10.1299/jbse.20-00017.

[27] N. Befrui *et al.*, "Vibroarthrography for early detection of knee osteoarthritis using normalized frequency features," *Medical & Biological Engineering & Computing*, vol. 56, no. 8, pp. 1499–1514, Aug. 2018, https://doi.org/10.1007/s11517-018-1785-4.